Proceedings of VSJ-SPIE98
December 6-9, 1998, Yokohama, JAPAN
AB082

Experimental and Computational Visualization of Vortex-Flame Interactions in an Opposed-Jet Burner

J.R. Gord,[1] J. M. Donbar,[1] G. J. Fiechtner,[2]
C.D. Carter,[2] V. R. Katta,[2] and J. C. Rolon[3]

[1] Air Force Research Laboratory, Wright-Patterson Air Force Base, OH 45433-7103, USA.
[2]Innovative Scientific Solutions, Inc., 2766 Indian Ripple Road, Dayton, OH 45440-3638, USA.
[3]Laboratoire d'Énergétique Moléculaire et Macroscopique, Combustion, École Centrale Paris, Grande Voie des Vignes, 92295 Châtenay-Malabry Cedex, France.

Abstract: The dynamic interaction of a laminar flame and a vortex is examined. The hydroxyl (OH) layer produced by the flame is imaged using planar laser-induced fluorescence (PLIF), and preliminary vortex-characterization data are acquired using acetone PLIF and digital, two-color particle-image velocimetry (PIV). The PIV and PLIF measurements of OH are performed simultaneously. The hydrogen-air flame is supported in a nonpremixed opposed-jet burner. The apparatus is found to produce highly repeatable events, making it ideal for studying the interaction of a flame and an isolated vortex. A distinct annular extinction of the OH layer is observed, in good agreement with previous computational modeling predictions for the apparatus.

Keywords: Visualization, Turbulence, Vortex, Flamelet, PLIF, PIV

1. Introduction

Recent results in numerical modeling combined with experimental measurements have led to important advances in the understanding of combustion. Numerous investigations have contributed to these advances, including a particular type of study in which the interaction of a laminar, nonpremixed flame and a vortex is examined. These efforts involve repeatable, carefully controlled conditions that are highly amenable to experimental study.

In recent computational calculations, Katta (Katta et al., 1998) predicted that during the interaction of a nonpremixed hydrogen-air flame and an isolated vortex, the extinction of the OH layer would occur in an annular pattern. Details of the numerical model are briefly discussed in this paper along with the associated prediction of an annular extinction. The experiments detailed in the present paper are performed to examine, in part, the validity of this prediction. Experimental results obtained with planar laser-induced fluorescence (PLIF) of OH are used to determine regimes in which the annular extinction occurs. The nonpremixed flame is supported by air and fuel in an opposed-jet burner. The fuel consists of hydrogen diluted with nitrogen. The amount of hydrogen in nitrogen is varied, along with the strength of the vortex. The temporal evolution of the vortex-flame interactions is imaged with the PLIF system.

Additional measurements are performed to characterize the vortices. First, acetone is seeded into the vortex, and its laser-induced fluorescence is detected. Second, particles are seeded into the flowfield and the scattering is used for digital, two-color particle-image velocimetry (PIV) measurements. Digital PIV measurements are made simultaneously with PLIF measurements of OH. Preliminary vortex-characterization results are discussed in this paper.

2. Background

Numerous experimental studies of the interaction dynamics of vortices and flames have been conducted, and many of these investigations employed two-dimensional imaging to study the interaction. For premixed flame fronts, most measurements have been made using two types of flames. Hertzberg et al. (1984) and Escudie (1988) conducted an experiment in which a Karman vortex street was produced using a cylindrical rod in a cross flow of premixed gases. A V-flame was supported behind a wire positioned downstream of the rod that produced the vortex street. Planar tomographic imaging was used to study the interaction of the vortex street and the flame. A similar interaction of a Karman vortex street and a flame was investigated by Lee et al. (1993) using PLIF imaging of OH and by Nye et al. (1996) using both OH PLIF and PIV. A disadvantage of using the vortex street is the difficulty in isolating a single vortex. Samaniego (1992a) developed a means of injecting an isolated line vortex through a horizontal slot in the wall of a vertical wind tunnel; this was pursued as a means of replacing the vortex street in experiments with V-flames. A year later, Samaniego (1992b) presented results on the interaction of a line vortex and a V-flame. Schleiren images of the time-dependent vortex-flame interaction along with CH emission data from the entire flame were presented. Nguyen and Paul (1996) also studied vortex-flame interactions using the Samaniego burner, reporting results of PLIF measurements of OH and CH radicals.

In a second type of study involving premixed combustion, Jarosinski et al. (1988) studied a flame that was ignited at one end of a tube of premixed gases. A vortex was injected at the other end of the tube. The interaction dynamics were then photographed using a mercury-xenon arc lamp and a rotating-drum streak camera with a rotating-disc shutter. Recently, Driscoll and co-workers produced an impressive series of papers concerning a similar vortex-flame facility in which PIV, OH PLIF, or a combination of these imaging techniques was applied (Driscoll et al., 1993; Driscoll et al., 1994, Mueller et al., 1995; Mueller et al., 1996; Mueller, 1996; Mueller et al., 1998; Roberts and Driscoll, 1991; Roberts, 1992; Roberts et al., 1992; Roberts et al., 1993; Sinibaldi et al., 1997; Sinibaldi et al., 1998).

Nonpremixed flames have also been the subject of experimental study. Rolon and co-workers (Renard et al., 1998a; Renard et al., 1998b; Rolon et al., 1995; Thevenin et al., 1996; Thevenin et al., 1998) recently developed an apparatus in which a vortex is injected into a flame supported between the nozzles of an opposed-jet burner. This geometry has numerous advantages. First, unlike the above geometries, a stationary nonpremixed flame can easily be produced and isolated. Second, the flame thickness can be varied by changing either the nozzle velocities or the spacing between the upper and lower burner nozzles. The device has also been extended to the study of vortices that interact with premixed opposed-jet flames (Renard et al., 1998a). Takagi and coworkers (Takagi et al., 1996; Yoshida and Takagi, 1998) performed planar Rayleigh-scattering measurements of temperature on a similar type of opposed-jet burner in which a small jet of fuel or air was injected using a micro-nozzle with an inner diameter of only 0.25 mm. Either a jet of air was injected from the air side of the diffusion flame or a jet of fuel was injected from the fuel side.

In a different class of measurements, Hsu et al., (1993) modulated the axial velocity of a laminar jet diffusion flame using a loud speaker to produce vortex-flame interactions. This apparatus was further studied by Hancock and coworkers (Hancock, 1996; Hancock et al., 1996; Hancock et al., 1997; Schauer, 1998; Schauer et al., 1998) using a number of techniques including reactive Mie scattering, PLIF, and digital PIV. These studies have provided large quantities of data for comparison with numerical-modeling predictions. A potential disadvantage of this burner is the complicated geometry (when compared to the above geometries, which involve completely isolated vortex injection) due to the convective velocity field associated with rotation of the vortex and translation of the flame zone (Hancock, 1996). In a similar type of study, Mueller and Scheffer (1998) recently performed OH PLIF measurements in a Wolfhard-Parker slot burner that was acoustically forced by loudspeakers on the side walls of the upstream fuel duct. PLIF imaging of acetone was used as a marker of the fuel.

More recently, Chen and Dahm (1997, 1998) developed a facility for generating a nonpremixed burning layer that wraps into a vortex ring. The facility permits experiments to be performed under conditions of both normal gravity and microgravity, allowing the study of the influence of buoyancy.

The experiments described in the present paper are based on the counterflow geometry of Rolon and co-workers, and the observations described below rely heavily on the progress outlined in their papers (Renard et al., 1998a; Renard et al., 1998b; Rolon et al., 1995; Thevenin et al., 1996; Thevenin et al., 1998). A fuel mixture of hydrogen and nitrogen permits the use of laser diagnostics in the absence of hydrocarbon interferences, and the reaction zone of these nonpremixed flames is generally much thicker than that for premixed flames. Hydrogen chemistry simplifies the numerical calculations that are the subject of comparison with experimental results.

3. Apparatus and Procedure

3.1 Burner Facility

A picture (a) and diagram (b) of the Rolon burner are shown in Figure 1. The flame is supported between upper and lower nozzles separated by 40 mm, each with an exit diameter of 25 mm. The fuel consists of hydrogen diluted with nitrogen and flows from the upper nozzle. Air flows from the lower nozzle. Unique to this type of apparatus is a tube with 5-mm inner diameter that is installed concentrically within the lower nozzle. This tube is attached to a cylinder that contains a piston which, in turn, is attached to an actuator. Feeding an appropriate current to the actuator causes a solenoid to force the piston upward abruptly, resulting in the emergence of a vortex from the tube. The vortex travels upward within the surrounding oxidizer flow. A flow of air is supplied to the vortex tube such that in the absence of a vortex, the exit velocity matches the velocity of the air from the surrounding nozzle. To minimize the impact of room-air disturbances, upper and lower guard flows of nitrogen are supported through outer nozzles, which are concentric with the respective upper and lower inner nozzles that support the flame.

The hydrogen, nitrogen-diluent, and oxidizer-air flows are furnished by mass-flow controllers with respective full-scale ranges of 20, 20, and 30 l/min. A continuous flow of air is provided to the vortex tube by a 5-l/min controller, while the guard flows for the upper and lower guard (outer) nozzles is furnished by two 50-l/min mass-flow controllers. The flow rates of the controllers are accurate to ± 1% of the full-scale range. The experiments have been repeated for six flame conditions, as summarized in Table I.

The vortex properties can be varied by changing the magnitude and the rise time of the current that is fed to the actuator. The impedance of the actuator ranges from 1 to 1.5 Ω, depending on the frequency content of the current. At full displacement, a current of up to 6 A is provided to the solenoid by a specially designed, high-speed power amplifier. This can result in considerable power consumption by the actuator if

the full-displacement condition is maintained for long periods. Consequently, an AC waveform is supplied by initial application of a negative potential, causing the piston to be withdrawn from the flame. The negative potential is applied for about 0.5 s to allow the flame to recover from this initial disturbance, as verified by digital, two-color PIV. The potential is then quickly changed to a positive value of the same magnitude with a carefully controlled rise time, τ_r. The strength of the vortex can be increased by increasing the current magnitude, which results in a larger volume of displaced fluid through the exit of the tube. Eventually, the maximum displacement of the solenoid is reached. In this case the vortex strength can be further increased using a smaller value of τ_r. The relationship among volume displacement, τ_r, and the vortex characteristics has been discussed in numerous papers, including those by Rolon et al. (1995), Roberts (1992), and Chen and Dahm (1997, 1998). The drive current for the solenoid is obtained by power amplifying the output of a digital arbitrary-waveform generator. This generator is operated at its maximum number of 10,000 quantized steps, resulting in a minimum step size of 0.1 ms. For all measurements discussed in this paper, τ_r is set at 10 ms.

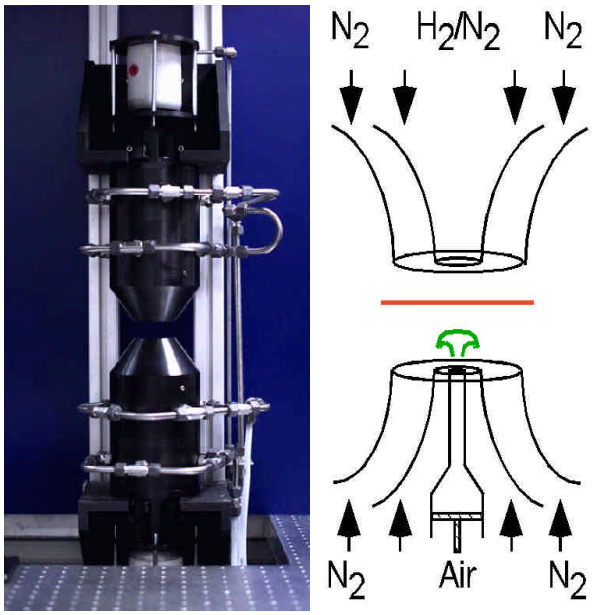

(a) (b)

Figure 1: (a) Digital photograph of opposed-jet burner. (b) Cross-sectional diagram of burner nozzles and piston.

Table I: Flow rates (l/min) at 21.5°C and 724 mm Hg for six flame conditions. X_{H2} is volume fraction of hydrogen in nitrogen diluent.

Gas	Flame					
	A	B	C	D	E	F
H_2	2.76	3.40	4.04	4.67	5.31	5.94
N_2 Diluent	17.1	17.1	17.1	17.0	17.0	16.9
X_{H2}	0.14	0.17	0.19	0.22	0.24	0.26
Air	11.2	11.2	11.2	11.2	11.2	11.2

Visualization of the vortex formation and propagation via acetone PLIF is accomplished using a vaporizer that is installed between the vortex tube and the mass-flow controller. A bypass valve allows adjustment of the acetone seeding level. Because the acetone changes the flame characteristics, these visualization studies are limited to nonreacting flows. When the acetone studies are not required, the acetone vaporizer is removed from the apparatus.

Seed particles are introduced into the burner flows when digital PIV measurements of the vortex velocity are performed. Three particle seeders are installed; one is placed after the air mass-flow controller, another after the vortex-air mass flow controller, and a third after the junction where the hydrogen and nitrogen gases are mixed. With the use of three seeders, each flow can be seeded with particles individually, or combinations of the different flowfields can be seeded. Each seeder contains hollow spherical ceramic particles with an approximate mean diameter of 2.4 μm. When PIV studies are not required, the seeders are removed from the apparatus.

3.2 Laser Diagnostics: OH PLIF Imaging

The PLIF system contains a frequency-doubled, Q-switched Nd:YAG laser that is used to pump a dye laser which, in turn, is frequency doubled. The UV radiation is directed through a telescope that is adjusted to produce a light sheet with a height that matches as nearly as possible the 40-mm burner separation. The resulting beam thickness is ~300 μm, which corresponds to the full width (defined as the distance between the locations of the 25% peak intensity points).

Hydroxyl radicals absorb the laser radiation at 281.3414 nm via the $R_1(8)$ transition of the (1,0) band in the A-X system. Fluorescence from the A-X (1,1) and (0,0) bands is detected at right angles through WG-295 and UG-11 colored-glass filters, using a 105-mm-focal-length f/4.5 UV lens. The resulting light is recorded on an intensified CCD camera with an intensifier gate width of 100 ns. CCD pixels are binned in 2x2 groups, resulting in an effective array size of 288 x 192 pixels, with an imaged area of 25.6 x 38.4 mm^2. The bottom of the image is 0.25-mm above the surface of the lower nozzle. A color table is used with a maximum value set to 95% of the maximum signal for all images taken at a given flame condition. The low-signal color is assigned by calculating the background noise and selecting a minimum value that is two standard deviations above this level. Therefore, in cases where "extinction" of the OH layer is observed, "extinction" refers to signal levels that fall below this minimum value and are, therefore, assigned the last color in the table. All images represent the signal collected during a single laser shot, and no smoothing of the resulting images is attempted.

In studies of vortex-flame interactions conducted by other investigators [see, for example, Najm et al., (1998)], LIF was applied as a marker of some other quantity such as heat release or burning rate. In the present experiments, the OH image is obtained for direct comparison with numerical computations of the OH distribution (Katta et al., 1998); therefore, no attempt is made to correlate the images with any other quantities, although it has recently been shown that the OH concentration may be a good indicator of flame extinction in this configuration (Renard et al., 1998b).

Acetone PLIF imaging is accomplished using the OH PLIF imaging system. Here, the UG-11 colored-glass filter is removed to permit collection of the acetone fluorescence.

3.3 Laser Diagnostics: Digital, Two-Color PIV

Measurements of the velocity field are carried out using digital, two-color PIV (Gogenini et al., 1998a; Gogenini et al., 1998b; Donbar, 1998). Here, a color digital CCD (Khosla, 1992) with an array of 3060 x 2036 pixels is used. A magnification of 78,368 pixels/m is employed, resulting in an imaged area of 26.0 x 39.0 mm^2. The color CCD camera and the intensified CCD array are aligned using a transparent mask printed with a graduated scale. Further alignment between images is performed after each experiment employing software; a transformation in two-dimensional space is applied to the PIV images relative to the PLIF images. Two lasers are used, with one PIV light sheet being produced by directly doubling the output of a Q-switched Nd:YAG laser (30 mJ/pulse at the test section). The remainder of this beam is used to pump the dye laser that is frequency doubled to excite OH fluorescence. The second PIV light sheet is produced by pumping a dye laser (employing DCM laser dye) with a second frequency-doubled, Q-switched Nd:YAG laser, resulting in laser radiation at 640 nm (40 mJ/pulse at the test section). The thickness of both the red and green light sheets is set to ~700 μm at the probe region. A digital delay generator is used to drive the timing of the two lasers such that the red pulses are delayed precisely with respect to the green ones. In the absence of a vortex, the underlying counterflow velocity field is probed with red pulses that are delayed by up to 1 ms with respect to the corresponding green pulses. For the fastest vortices studied, the delay between red and green pulses is reduced to 10 μs. The camera shutter is set to open for 1/15 s to permit both laser pulses to be detected by the color CCD. Most of the flame emission and light from other devices in the laboratory (monitors, etc.) is greatly attenuated by the shutter.

Velocity vectors are calculated using the correlation software described by Gogenini et al., (1998a). A correlation area of 128 x 128 pixels is used in the calculation, corresponding to a correlation area of 0.269 cm^2 and a spatial resolution of 1.6 mm. In these preliminary studies, the main interest in digital PIV measurements is to obtain the propagation velocity of the vortex, and this correlation area is acceptable for such purposes. We have also obtained acceptable results using correlation areas as small as 32 x 32 pixels, which will be utilized in future studies in which quantities such as strain will be calculated. Neighboring correlation boxes are overlapped by 75%, resulting in a velocity field with an area containing 95 x 60 vectors, or 5700 total vectors over the area of the color CCD. In some portions of each image, a small percentage of errant vectors results from low seed levels, scattering of light into the camera, flame emission, and other effects. Because the vortex-flame interactions are repeatable, digital PIV images can be recorded until an image with an extremely small percentage of incorrect vectors is obtained. For this reason, nearly 15 gigabytes of digital color image data were acquired.

Characterization of vortices is illustrated in Figure 2; a single, idealized vortex ring is superimposed over an axisymmetric cylindrical coordinate system using the coordinates z and u to illustrate the forward position and velocity, respectively. The coordinates r and v represent the radial position and velocity, respectively. In this coordinate representation, the vorticity simplifies to

$$\vec{z} = \Delta \times \vec{V} = \frac{\partial v}{\partial z} - \frac{\partial u}{\partial r}. \qquad (1)$$

In these preliminary studies, evaluation of the derivatives in Eq. (1) is carried out without smoothing of the velocity field. Because this can cause amplification of noise, future calculations will be performed using an appropriate smoothing algorithm (Luff et al., 1996; Luff et al., 1998). When the velocity field represents the final desired result from reduction of digital PIV images, it is common to filter out incorrect vectors; this results in “holes” in the field that must be filled using a variety of techniques such as interpolation (Gogineni et al., 1998b). However, the resulting interpolated holes will represent a source of significant error in vorticity computations (Luff et al., 1996; Luff et al., 1998). Therefore, images with more than a few holes are discarded before attempts are made to compute the vorticity. In the future, an optimum method of computing the velocity field will be implemented to reduce the uncertainty in vorticity produced by the holes. Before images of vorticity are plotted, a 3 x 3 smoothing function, that is provided with the commercially available Transform® software, is applied four times. In these preliminary studies, the resulting images are used to examine the relative distribution of vorticity as a vortex propagates upward from the lower nozzle. In future studies in which the influence of the flame on the vorticity will be examined and quantitative vorticity information extracted, a more accurate method of computing and displaying the vorticity will be implemented (Luff et al., 1996; Luff et al., 1998).

The vortex circulation is computed using the integral over the contour shown in Figure 2 (Sullivan et al., 1973a; Sullivan et al., 1973b), yielding (Fox and MacDonald, 1985; Daily and Harleman, 1966; Luff et al., 1996; Luff et al., 1998)

$$\Gamma = \oint_C \vec{V} \bullet d\vec{s} = \sum_i \sum_j \vec{V}_{ij} \bullet \vec{s}_{ij} = \sum_i \sum_j z_{ij} A_{\text{cell}} \qquad (2)$$

where C represents a contour box whose sides are drawn along lines where the vorticity remains below ~10% of its peak value (found at the core). The line-integral method (first double summation) and the vorticity-integral method (second double summation) are found to agree within 20%. To confirm the choice of contour and the integration process, the integration is performed over each side of the vortex depicted in Figure 2, and the resulting sum is determined to approach zero.

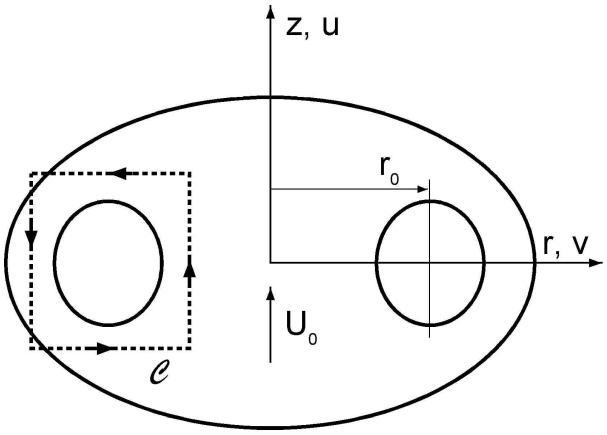

Figure 2. Coordinate system and integration contour used during computation of vortex properties (Daily and Harleman, 1966; Fox and MacDonald, 1985; Sullivan et al., 1973a; Sullivan et al., 1973b).

3.4 Synchronization and Timing

Precise synchronization of several experimental events is required, including vortex generation and propagation, production of laser pulses, and activation of the camera shutter or intensifier. Figure 3 contains a block diagram of the synchronization scheme.

Because the Nd:YAG lasers are designed to operate at a nominal repetition rate of 10 Hz, the experimental sequence must be synchronized to a 10-Hz master clock that drives the flash lamps and the Pockels cells of the lasers. To trigger the lasers, the clock sends two signals—one traveling to a 50-Ω power combiner and then to the laser digital delay generator (DDG). The 10-Hz clock also provides a TTL signal to one of two inputs of a coincidence unit. The second input of this unit is driven by a TTL pulse from the PLIF camera controller. The coincidence unit outputs a pulse only when pulses from both the 10-Hz clock and the PLIF camera controller are present. When a vortex-flame event is initiated using a personal computer, the PLIF camera controller outputs a pulse ~1.3 s in duration. The corresponding output of the coincidence unit is a 1.3-s envelope of TTL pulses separated by 100 ms. The first pulse in this envelope triggers a master DDG, synchronizing it with the 10-Hz clock and the laser pulse train. This DDG triggers an arbitrary-waveform generator (AWG) that outputs a 1-s waveform; this waveform is amplified and fed to the piston actuator to generate a vortex. Approximately 0.5 s after the AWG waveform is initiated, the vortex is fired; therefore, five laser pulses are generated during the time between computer initiation and the vortex-flame interaction.

When the DDG is externally triggered, the jitter between the trigger and a DDG output pulse is 60 ps plus the output delay divided by 10^8. Over the 0.5-s period between the first and fifth laser pulses, this corresponds to a jitter of 5.06 ns. The 10-Hz-clock jitter specifications are not nearly so good. The jitter between clock outputs is one part in 10,000, corresponding to a jitter of 50 μs over the same 0.5-s period. Attempting to synchronize the piston with the clock severely limits the temporal resolution available to "freeze" vortex-flame events in time and requires an intensifier gate width significantly larger than 50 μs. The master DDG is, therefore, configured to trigger the fifth laser pulse preemptively. A delayed pulse from the master DDG arrives at the 50-Ω power combiner just before the fifth pulse in the clock pulse train, preemptively triggering the laser(s). If no initiation pulse is output from the computer, the laser(s) are triggered by the 10-Hz clock as usual. This approach reduces the jitter in the timing of the fifth laser pulse from 50 μs to ~5 ns while maintaining the nominal 10-Hz repetition rate required by the lasers.

Other outputs of the master DDG are suitably delayed and directed to the image detectors. For PIV experiments, the width of a TTL pulse is adjusted using a gate generator, which closes a relay to trigger the digital PIV camera system. For simultaneous PLIF experiments, another master-DDG output triggers a pulse generator which, in turn, activates the intensifier of an ICCD camera.

The scheme depicted in Figure 3 provides precise control of the relative timing between the laser diagnostics and the vortex-flame event. To explore the temporal evolution of the event, data are captured utilizing the following phase-locked timing sequence: 1) an image is recorded, 2) the delay between vortex production and the laser/camera events is adjusted, and 3) another vortex is initiated and a second image recorded. This process is repeated to acquire numerous images, obtained at increasing delays; then an animation is created by assembling the individual images in temporal order. Effective temporal separation between images is selected between 10 and 200 μs, depending on the time scale of the event under study. The resulting animations are a testament to the high degree of repeatability achievable with this apparatus.

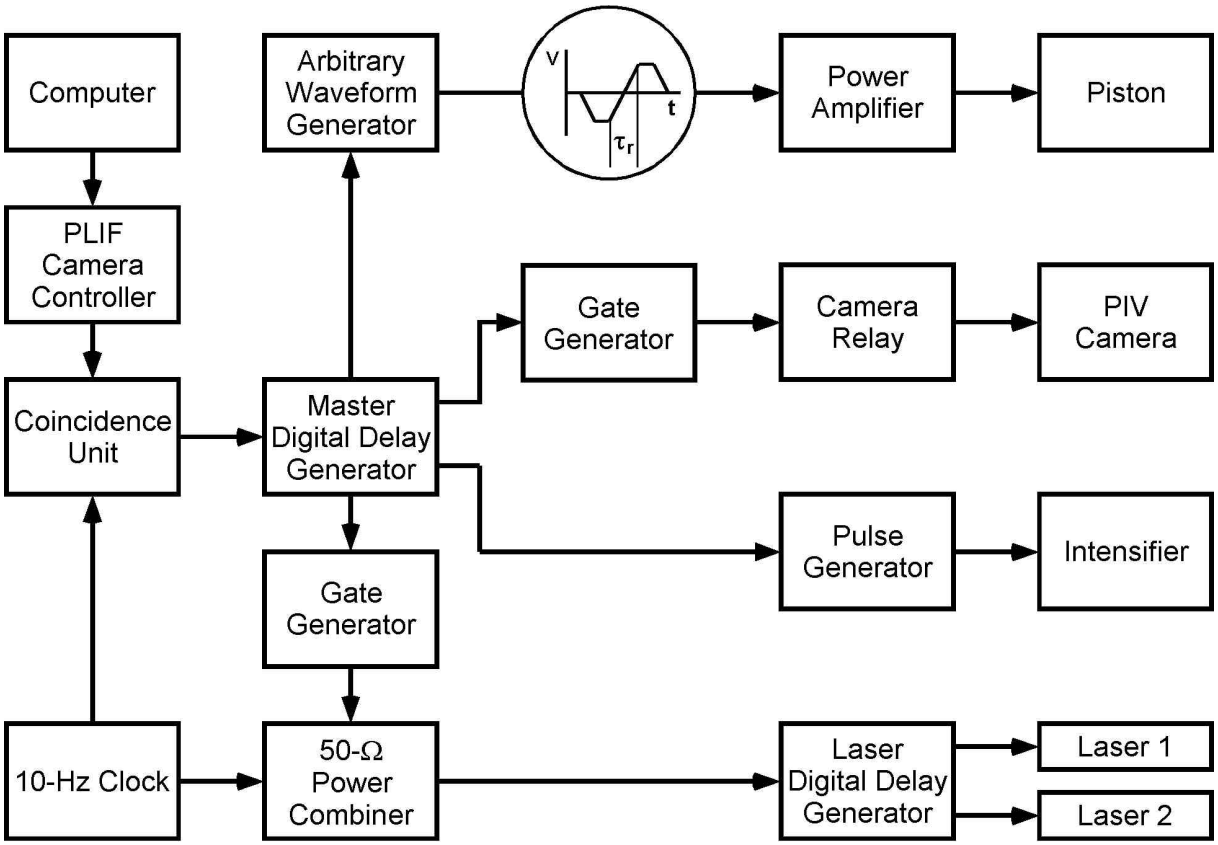

Figure 3: Diagram of electronic timing connections for simultaneous OH PLIF and digital PIV measurements.

3.5 Computational Model

Time-dependent, axisymmetric Navier-Stokes equations written in cylindrical coordinates are solved along with species- and energy-conservation equations. A detailed chemical kinetics model containing thirteen species (H_2, O_2, H, O, OH, H_2O, HO_2, H_2O_2, N, NO, NO_2, N_2O, and N_2) is used to describe hydrogen-air combustion. Seventy-four reactions among the constituent species are used, with rate constants obtained from Frenklach et al. (1995). Temperature- and species-dependent property calculations are also incorporated into the model; the enthalpy of each species is calculated from polynomial curve fits that were developed for the temperature range 300-5000 K. The viscosity and the thermal conductivity of individual species are estimated from the Chapman-Enskog collision theory, and the mixture properties are obtained employing Wilke's semi-empirical formula. The effective binary diffusion coefficient of the individual species in the local mixture is calculated using molecular dynamics and Lennard-Jones potentials.

The governing equations are integrated on a nonuniform staggered-grid system. An orthogonal grid with rapidly expanding cell sizes in the axial and the radial directions is employed. The finite-difference forms of the momentum equations are obtained using an implicit QUICKEST scheme (Leonard, 1979; Katta et al., 1994), and those of the species and energy equations are obtained using a hybrid scheme of upwind and central differencing. At every time step, the pressure field is calculated by solving the pressure Poisson equations simultaneously and utilizing the LU matrix decomposition technique. Calculations are made using a non-uniform 301 x 121 mesh system with a spacing of 0.1 mm in both the axial and radial directions. The fuel and air jets are assumed to have velocities of 0.69 and 0.5 m/s, respectively, and the hydrogen-to-nitrogen ratio used for the fuel jet is 0.38. The vortex is modeled by forcing 2.2 cm^3 of air through the exit of

a nozzle with an exit velocity that increases linearly at a rate of 10^3 m/s/s. Further details are given by Katta et al., (1998).

4. Results and Discussion

4.1 Vortex Characterization

The series of acetone images in Figure 4 is typical of the sequential images used to measure the vortex-propagation velocity for a given amplitude and rise time of the solenoid drive current. The six images in the figure are selections from a sequence of fifty images, each delayed by 100 μs relative to the previous one. If the location of the flame front in the absence of a vortex is known, the acetone-PLIF image sequence can be used to estimate the velocity of the vortex at this location. In this case, the propagation velocity is ~5 m/s.

Recently, characterization of vortex properties has been initiated using PIV, which is accomplished simultaneously with OH PLIF. Digital, two-color PIV measurements are readily made when the flame is burning, offering a significant advantage over the acetone-PLIF measurements of the vortex propagation velocity. Figure 5 shows the scattering signal obtained when the vortex-tube flow is seeded with a slightly higher particle density than that produced by the upper- and lower-

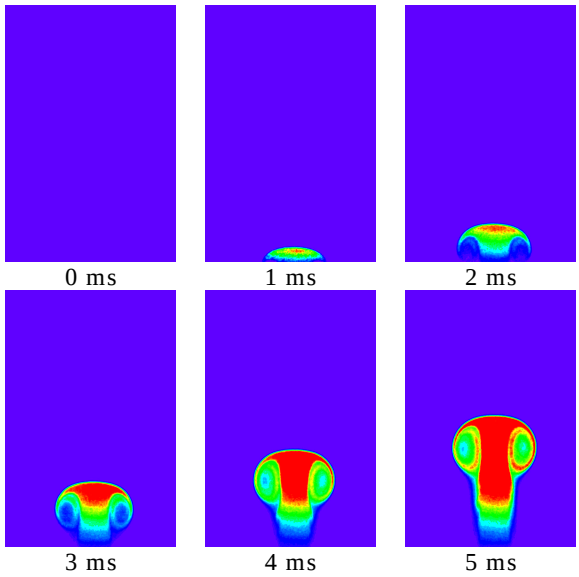

Figure 4: Acetone-PLIF images of vortex.

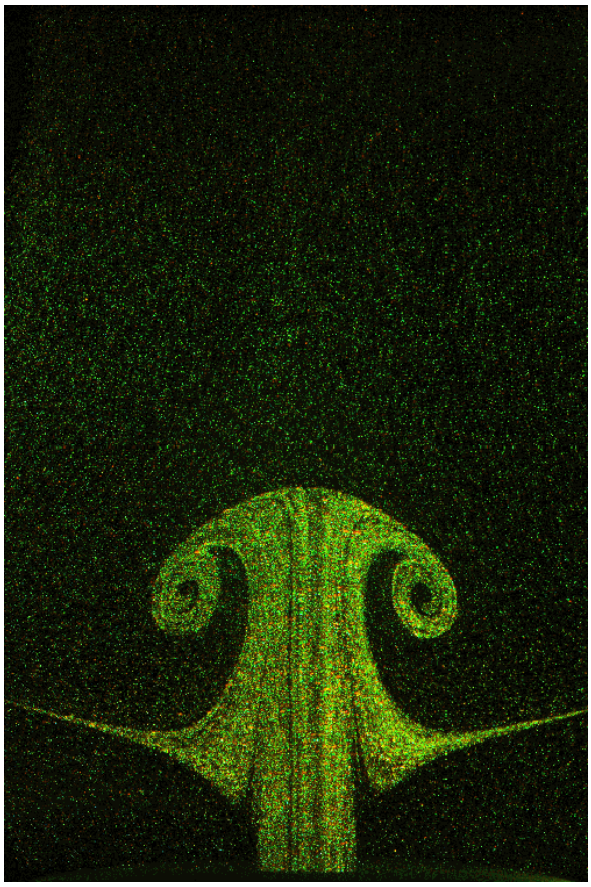

Figure 5: Scattering from particles in vortex flow.

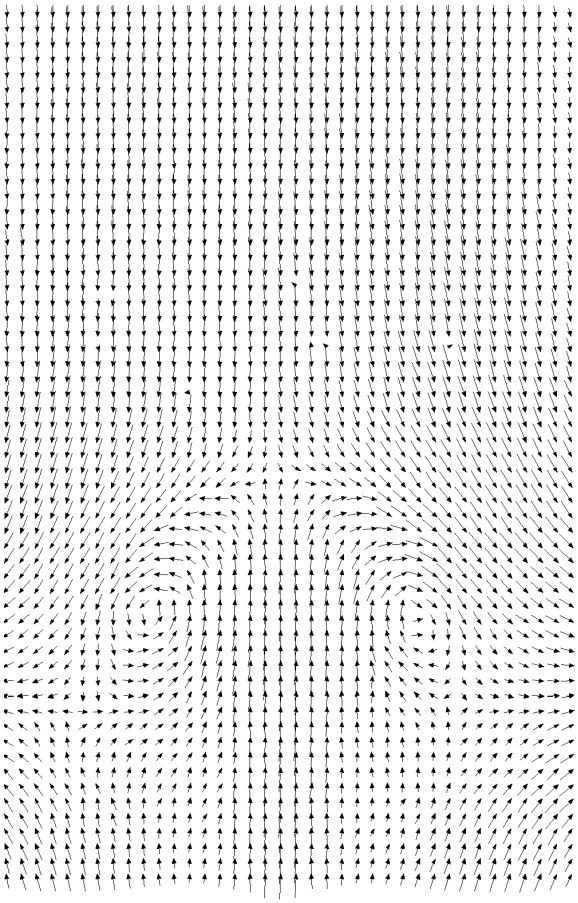

Figure 6: Vectors calculated from PIV image of Figure 5.

burner. The corresponding set of vectors is shown in Figure 6. The maximum vector length in the forward direction yields a propagation velocity of 0.77 m/s in this case.

It is now well known that the a strained field can have significant influence on the history of a vortex (Brickman and Ruddick, 1990; Dritchel, 1989; Legras and Dritchel, 1993; Mariotti et al., 1994; Trieleng et al., 1997; Trieleng et al., 1998). Therefore, it is extremely important that the vortices be characterized. Three different vortices are shown in Figure 7 by their respective vorticity fields, including a "weak," an "intermediate," and a "strong" vortex in row (a), (b), and (c), respectively. The weak vortex has a circulation of ~76 cm^2/s and an initial propagation velocity of 1 m/s. However, the propagation velocity of this vortex slows to only 0.6 m/s by the fifth frame (labeled "50 ms"). Meanwhile, the separation between cores is $2r_0$=7 mm in the first frame (labeled "0 ms") and increases to nearly 15 mm in the fifth frame.

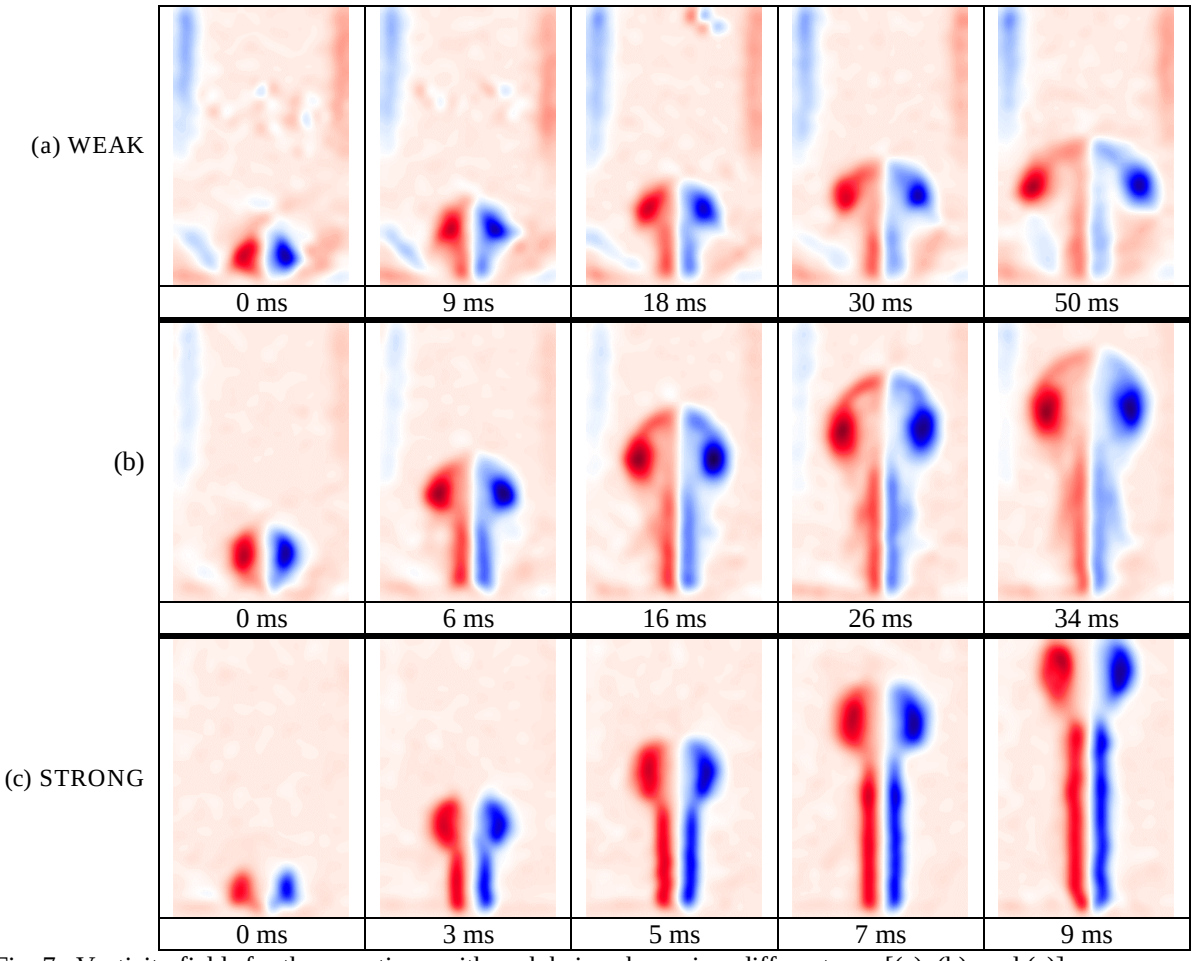

Fig. 7. Vorticity fields for three vortices, with each being shown in a different row [(a), (b), and (c)].

In contrast, the intermediate vortex shown in row (b) of Figure 7 has a circulation of 170 cm^2/s and an initial propagation velocity of 2.2 m/s. By the time the vortex reaches the position shown in the fifth frame of row (b), the propagation velocity has decreased to 1.8 m/s. The intermediate vortex shown in the first frame of row (b) has a core seperation of $2r_0$=7.8 mm, which increases to ~12 mm by the fifth frame of row (b). Row (c) contains the time-resolved vorticity field for a "strong" vortex, which has a circulation of 1200 cm^2/s. This vortex has a propagation velocity of 8.4 m/s in the first frame. The velocity increases to a value of 10 m/s in the fourth frame and then decreases to 9.5 m/s in the fifth frame of row (c). The strong vortex has a core separation of $2r_0$=8 mm in the first frame, and the diameter grows to a value of ~10.5 mm by the fifth frame of row (c). The strong vortex is observed to enter the upper-burner nozzle after the fifth frame. Care must be taken when attempting to generate a vortex that is stronger than case (c) since a three-dimensional lobe structure may result (Widnall, 1975).

Vortex characterization is also essential in choosing the amount of volume that is discharged from the piston/cylinder when generating a vortex. For an equivalent cylindrical volume that emanates from a nozzle having length L and diameter D, Gharib et al., (1998) have shown that the maximum circulation that a vortex ring can attain is reached for L/D at ~4 and that for larger ratios, additional trailing vortex rings form. For the present 0.5-cm nozzle, the volume that a vortex can contain as estimated from the results of Gharib et al., (1998) is ~0.4 cm^3. The present vortex generator can sweep a maximum volume of ~3 cm^3, for

a maximum attainable L/D ratio of ~30. An example of the consequences of overfilling the vortex is shown in Figure 8, which contains Mie scattering images from PIV particles as viewed with the color digital camera. The first frame (labelled "0 ms") corresponds to the instance in which the vortex reaches the flame and begins to induce flame curvature. After 2 ms, when this vortex has clearly passed the initial flame-front position, a second vortex has obviously formed. After another 2 ms, a third vortex is observed, and after 5 ms, the second vortex is observed to overtake the leading vortex and reach the flame front. This vortex leapfrogging process is found to be highly repeatable and, in future studies, may also prove valuable because of the unique curvature and strain regions formed by these events.

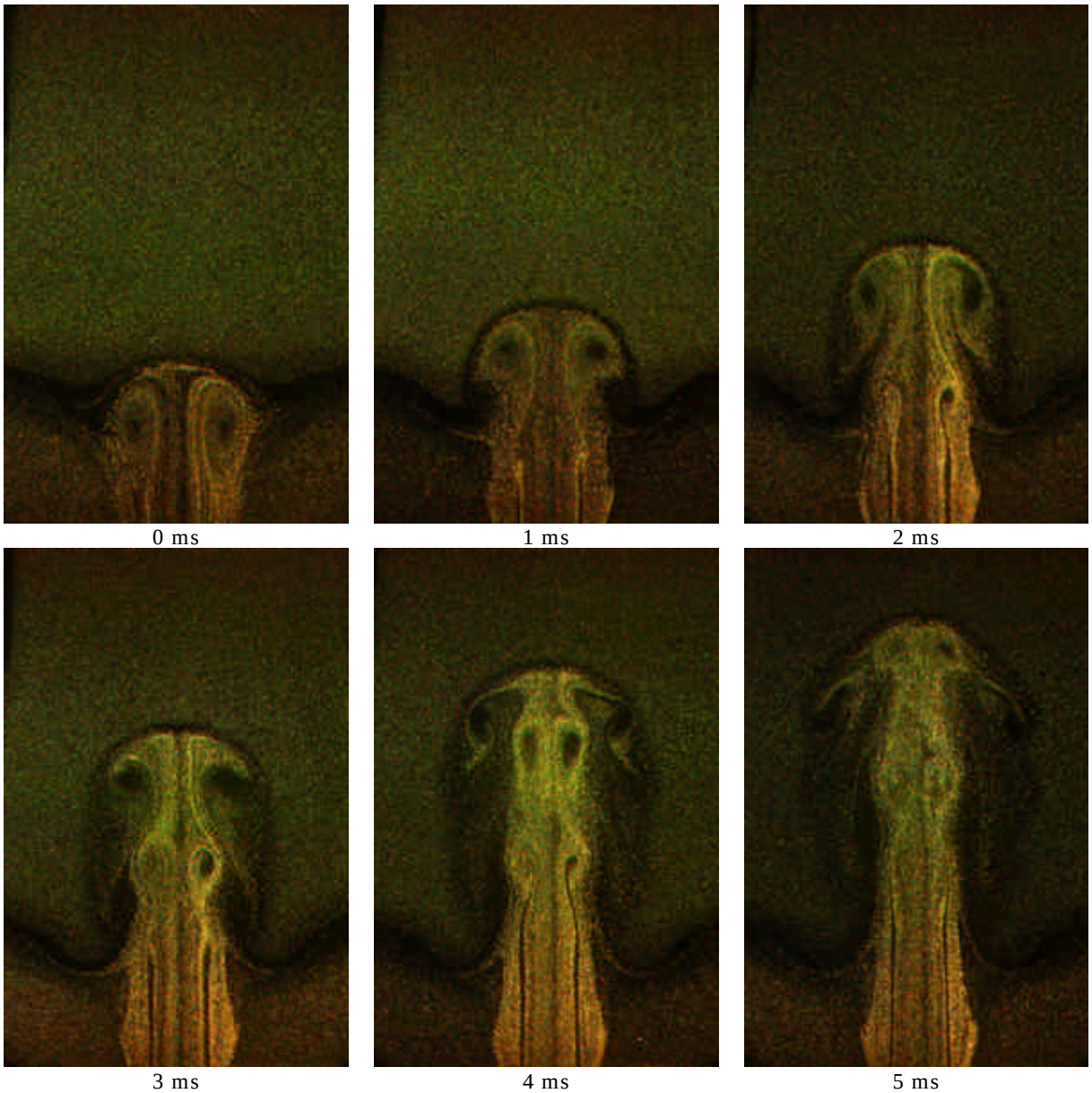

Figure 8: Mie scattering images of an attempt to overfill the vortex. Secondary and tertiary vortices are formed.

4.2 Regimes of Vortex-Flame Interaction

The PLIF images of OH shown in Figure 9 correspond to a vortex-flame interaction in which extinction of the OH layer is absent. Initially, the vortex creates a small dent in the flame, and this dent begins to grow. Eventually the flame nearly surrounds the advancing vortex as it approaches the upper nozzle. In the later interaction stages, the OH PLIF signal level is observed to increase by more than a factor of five over the levels observed without a vortex. The increased signal level is indicated by the light colors in the frames of Figure 9. This change in OH signal level is thought to indicate enhanced burning. For this particular example, the flow rates of Flame D in Table I are used.

The images of Figure 10 correspond to Flame E in Table I and a vortex that is considered to be "strong." Extinction of the OH layer takes place in an annular pattern around the sides of the vortex, leaving a burning layer at its leading edge. After extinction, the isolated island of flame burns away, and the vortex travels upward toward the other nozzle. The flame follows the vortex, traveling up the stem. As the flame overtakes the vortex, it wraps up and turns in upon itself. An additional effect can be seen in flames that exhibit the annular extinction if the vortex strength is slightly decreased: The isolated island at first shrinks in size, but does not completely disappear; it then begins to grow, and burns back around the vortex as it propagates upward. This process is demonstrated in the images of Figure 11.

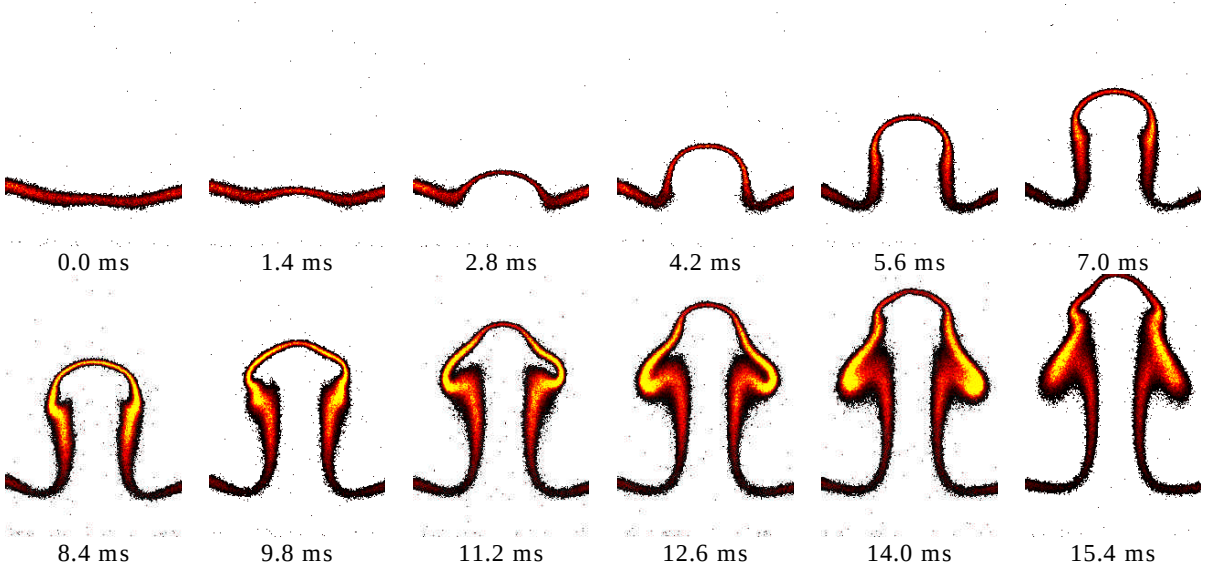

Fig. 9. OH PLIF images when the OH layer remains intact.

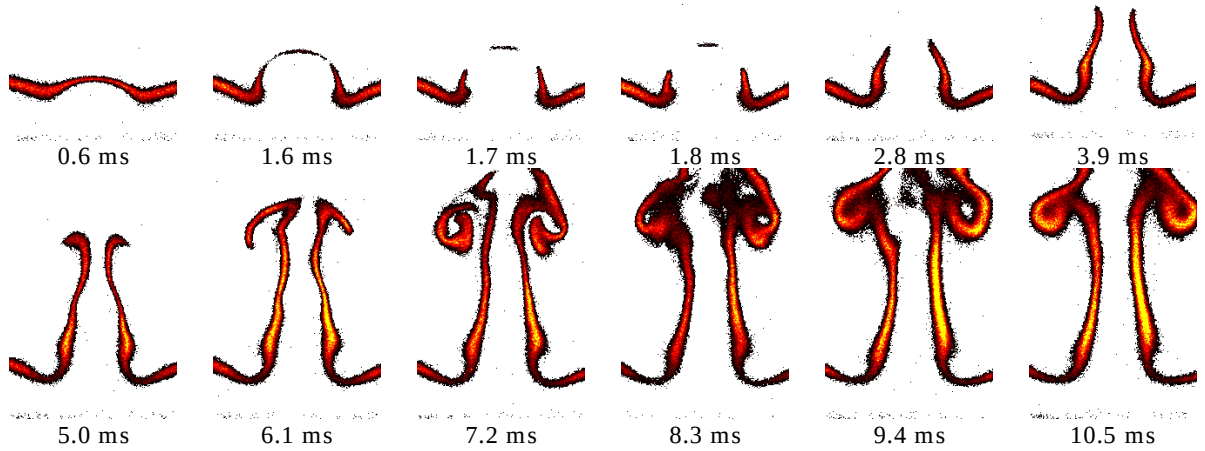

Figure 10: Sequence of images before and after annular extinction of the OH layer.

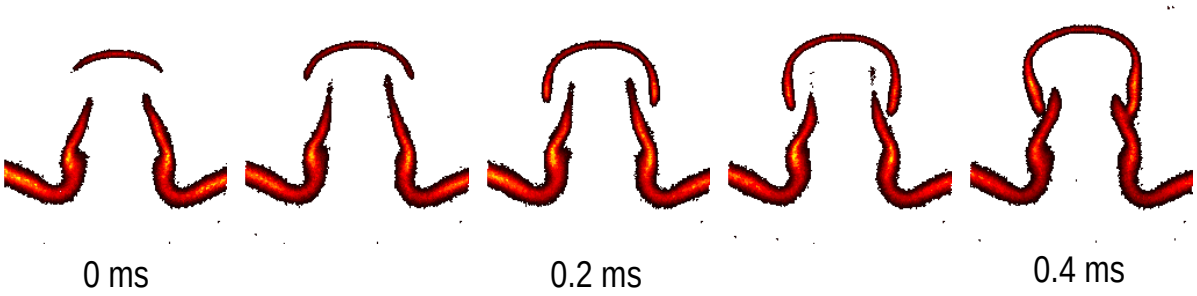

Figure 11. Sequences of images in which the island of flame that is isolated after the annular break in the OH layer begins to grow. Eventually the isolated island recombines with the sides of the flame.

4.3 Animations of Experimental Results

Animations are made from sequences of experimental images. Animation AB082_1 corresponds to the acetone PLIF results of Figure 4. Images are separated by a delay of 100 μs. Animation AB082_2 corresponds to the OH PLIF results of Figure 9. Animation AB082_3 corresponds to the OH PLIF results of Figure 10. The delay between images in each case is 100 μs. To focus on the regime of annular extinction, the measurements corresponding to Figure 10 were repeated using a delay of only 10 μs. The corresponding results are shown in Animation AB082_4. The 50 frames in this animation were obtained in sequential order; images were not reshuffled to make the animation smoother. As demonstrated in Animation AB082_4, the repeatability of the Rolon burner is exceptional.

4.4 Computational Results

A typical computational result is shown in Figure 12, which contains images of the streakline, temperature, OH, and H fields. The annular decrease in the OH layer is quite similar to the experimental results shown in Figure 10. In fact, the numerical results were obtained before the experiments were initiated, attesting to the utility of the code. Detailed analysis of the numerical results reveal that the strain rate in the annular region is equal to or lower than that at the stagnation line, and the flame curvature increases significantly in the annular region where the break in the OH layer appears. Based on these observations, it is postulated that the annular mechanism results from the combined effect of preferential diffusion and flame curvature. Indeed, Yoshida and Takagi (1998) have found that, in nonpremixed counterflow flames of hydrogen and air into which a microjet is injected, preferential difffusion can cause enhanced H_2 concentrations in regions with concave curvature, greatly influencing extinction and reignition processes.

5. Conclusions and Future Research

The apparatus of Rolon and co-workers (Renard et al., 1998a; Renard et al., 1998b; Rolon et al., 1995; Thevenin et al., 1996; Thevenin et al., 1998) has been implemented to study of the interaction of a vortex and a flame. PLIF measurements of acetone and digital, two-color PIV have been applied to characterize the vortices injected into the opposed-jet flow. PLIF images of OH have been used to observe the dynamics of the interaction of the vortex and the flame. An annular break in the OH layer has been observed in excellent agreement with the numerical computations of Katta (Katta et al., 1998).

Future work will be directed toward the understanding of phenomena such as the annular extinction. A variety of parameters can be studied, such as extended ranges of nitrogen dilution in hydrogen, various flame-thickness regimes and vortex sizes, and different fuels. To aid in these studies, simultaneous OH PLIF and digital, two-color PIV will continue to be employed, along with measurements of the temperature field.

Acknowledgements

The authors thank Mr. K. D. Grinstead, Jr., for technical assistance in setting up the experiments. The authors also acknowledge the advice of Drs. L. P. Goss, S. Gogineni, J. Estevadeordal, M. A. Linne, and Mr. T. Drouillard concerning the reduction of two-color PIV data. The authors thank Dr. R. D. Hancock and Mr. I. Vihinen for assistance in assembly and construction of the burner. The authors also acknowledge Mr. P.-H. Renard and Drs. R. D. Hancock, W. M. Roquemore, V. R. Katta, and K.-Y. Hsu for the stimulating discussions of vortex-flame dynamics. Finally, the authors wish to thank Ms. M. M. Whitaker for editorial comments. This work is supported by U. S. Air Force Contracts F33615-95-C-2507 and F33615-97-C-2702.

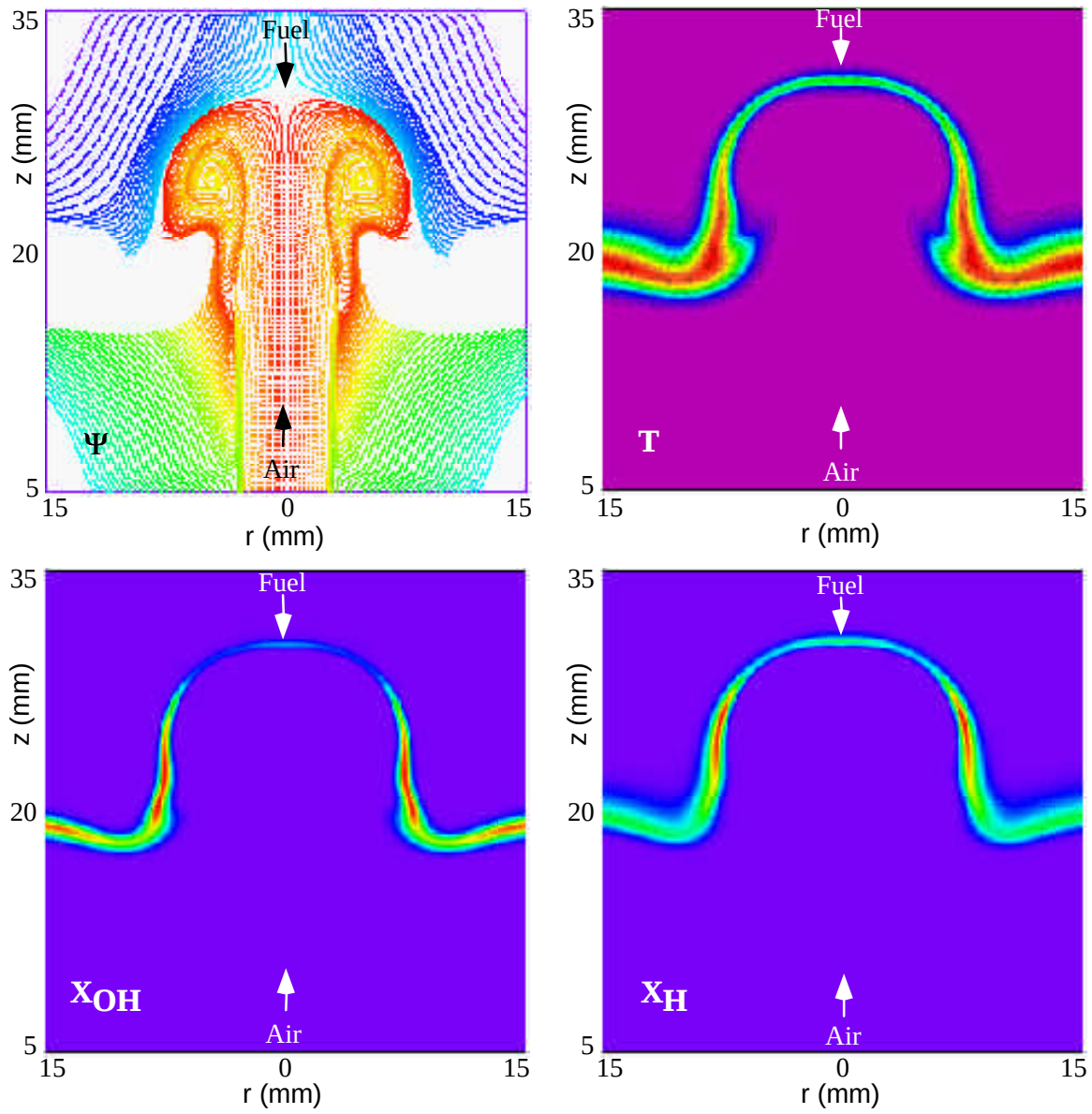

Figure 12. Computational result of Katta (Katta et al., 1998). The image in the upper left hand corner depicts a particle trace of the streamlines. The image in the upper right hand corner shows the temperature field, while the lower left and right images contain the OH and H fields, respectively.

References

Brickman, D., and Ruddick, B., 1990, "The Behavior and Stability of a Lens in a Strain Field," *Journal of Geophysical Research*, Vol. 95, No. C6, pp. 9657-9670.

Chen, S.-J., and Dahm, W. J. A., 1997, "Vortex Ring/Diffusion Flame Interactions in Microgravity Conditions," Proceedings of the *Fourth International Microgravity Combustion Workshop*, Cleveland, OH, pp. 191-196. NASA Conference Publication No. 10191.

Chen, S.-J., and Dahm, W. J. A, 1998, "Diffusion Flame Structure of a Laminar Vortex Ring Under Microgravity Conditions," accepted for publication in *Twenty-Seventh Symposium (International) on Combustion*, The Combustion Institute, Pittsburgh.

Daily, J. W., and Harleman, D. R. F., 1966, "Fluid Dynamics," Addison-Wesley Publishing, Reading, MA.

Donbar, J. M., 1998, "Reaction Zone Structure and Velocity Measurements in Permanently Blue Nonpremixed Jet Flames," Ph.D. Dissertation, University of Michigan, Ann Arbor.

Driscoll, J. F., Sutkus, D. J., Roberts, W. L., Post, M. E., and Goss, L. P., 1993, "The Strain Exerted by a Vortex on a Flame – Determined from Velocity Field Images," AIAA Paper No. 93-0362.

Driscoll, J. F., Sutkus, D. J., Roberts, W. L., Post, M. E., and Goss, L. P., 1994, "The Strain Exerted by a Vor-

tex on a Flame – Determined from Velocity Field Images," *Combustion Science and Technology*, Vol. 4/6, pp. 213-229.

Dritschel, D. G., 1989, "Strain-Induced Vortex Stripping," in *Mathematical Aspects of Vortex Dynamics*, R. E. Caflisch, ed., SIAM, Philadelphia, PA, pp. 107-119.

Escudie, D., 1988, "Stability of a Premixed Laminar V-Shaped Flame," *Progress in Astronautics and Aeronautics*, Vol. 113, pp. 215-239.

Fox, R. W., and McDonald, A. T., 1985, "Introduction to Fluid Mechanics," John Wiley & Sons, New York.

Frenklach, M., Wang, H., Goldenberg, M., Smith, G. P., Golden, D. M., Bowman, C. T., Hanson, R. K., Gardiner, W. C., Lissianski, V., 1995, *Gas Research Institute Technical Report* No. GRI-95/0058.

Gharib, M., Rambod, E., and Shariff, K., 1988, "A Universal Time Scale for Vortex Ring Formation," *Journal of Fluid Mechanics*, Vol. 360, pp. 121-140.

Gogineni, S., Goss, L. P., and Roquemore, W. M., 1998a, "Manipulation of a Jet in a Cross Flow," *Experimental Thermal and Fluid Science*, Vol. 16, pp. 209-219.

Gogineni, S., Goss, L., Pestian, D., and Rivir, R., 1998b, "Two-Color Digital PIV Employing a Single CCD Camera," *Experiments in Fluids*, in press.

Hancock, R. D., 1996, "Laser Diagnostic Investigation of the Structure of Steady and Driven Hydrogen Jet Diffusion Flames," Ph.D. Dissertation, University of Illinois, Urbana.

Hancock, R. D., Schauer, F. R., Lucht, R. P., Katta, V. R., and Hsu, K. Y., 1996, "Thermal Diffusion Effects and Vortex-Flame Interactions in Hydrogen Jet Diffusion Flames," *Twenty-Sixth Symposium (International) on Combustion*, The Combustion Institute, Pittsburgh, pp. 1087-1093.

Hancock, R. D., Schauer, F. R., Lucht, R. P., and Farrow, R. L., 1997, "Dual-Pump Coherent Anti-Stokes Raman Scattering (CARS) Measurements of Nitrogen and Oxygen in a Laminar Jet Diffusion Flame," *Applied Optics*, Vol. 36, No. 15, pp. 3217-3226.

Hertzberg, J. R., Namazian, M., and Talbot, L., 1984, "A Laser Tomographic Study of a Laminar Flame in a Karman Vortex Street," *Combustion Science and Technology*, Vol. 38, No. 3/4, pp. 205-216.

Hsu, K. Y., Chen, L. D., Katta, V. R., Goss, L. P., and Roquemore, W. M., 1993, "Experimental and Numerical Investigations of the Vortex-Flame Interactions in a Driven Jet Diffusion Flame," AIAA Paper No. 93-0455.

Jarosinski, J., Lee, J. H. S., and Knystautas, R., 1988, "Interaction of a Vortex Ring and a Laminar Flame," *Twenty-Second Symposium (International) on Combustion*, Pittsburgh, pp. 505-514.

Katta, V. R., Goss, L. P., and Roquemore, W. M., 1994, "Numerical Investigations of Transitional H_2/N_2 Jet Diffusion Flames," *AIAA Journal*, Vol. 32, No. 1, pp. 84-94.

Katta, V.R., Carter, C. D., Fiechtner, G. J., Roquemore, W. M., Gord, J. R. and Rolon, J. C., 1998, "Interaction of a Vortex With a Flat Flame Formed Between Opposing Jets of Hydrogen and Air," accepted for publication in *Twenty-Seventh Symposium (International) on Combustion*, The Combustion Institute, Pittsburgh.

Khosla, R. P., 1992, "From Photons to Bits," *Physics Today*, Vol. 45, No. 12, pp. 42-49.

Lee, T.-W., Lee, J. G., Nye, D. A., and Santavicca, D. A., 1993, "Local Response and Surface Properties of Premixed Flames During Interactions with Karman Vortex Streets," *Combustion and Flame*, Vol. 94, No. 1/2, pp. 146-160.

Legras, B., and Dritschel, D. G., 1993, "Vortex Stripping and the Generation of High Vorticity Gradients in Two-Dimensional Flows," *Applied Scientific Research*, Vol. 51, pp. 445-455.

Leonard, B. P., 1979, "A Stable and Accurate Convective Modeling Procedure Based on Quadratic Upstream Interpolation," *Computer Methods in Applied Mechanics and Engineering*, Vol. 19, pp. 59-98.

Luff, J. D., Rompage, A. M., Linne, M. A., and Hertzberg, J. R., 1996, "Uncertainties Associated with the Post-Processing of 2-D Particle Image Velocimetry (PIV) Velocity Data of Unsteady Flow Fields," presented at the *Spring Meeting of the Western States Section of the Combustion Institute*, Tempe, AZ, March, 1996. Paper No. WSS 96S-005.

Luff, J. D., Drouillard, T., Rompage, A. M., Linne, M. A., and Hertzberg, J. R., 1998, "Experimental Uncertainties Associated with Particle Image Velocimetry (PIV) Based Vorticity Algorithms," to appear in *Experiments in Fluids*, Vol. 25.

Mariotte, A., and Legras, B., 1994, "Vortex Stripping and the Erosion of Coherent Structures in Two-Dimensional Flows," *Physics of Fluids*, Vol. 6, No. 12, pp. 3954-3962.

Mueller, C. J., Driscoll, J. F., Sutkus, D. J., Roberts, W. L., Drake, M. C., and Smooke, M. D., 1995, "Effect of Unsteady Stretch Rate on OH Chemistry During a Vortex-Flame Interaction: To Assess Flamelet Models," *Combustion and Flame*, Vol. 100, No. 1/2, pp. 323-331.

Mueller, C. J., Driscoll, J. F., Ruess, D. L., and Drake, M. C., 1996, "Effects of Unsteady Stretch on the Strength of a Freely-Propagating Flame Wrinkled by a Vortex," *Twenty-Sixth Symposium (International) on Combustion*, The Combustion Institute, Pittsburgh, pp. 347-355.

Mueller, C. J., 1996, "Measurements of Vortex-Flame Interaction Dynamics and Chemistry," Ph.D. Dissertation, University of Michigan, Ann Arbor.

Mueller, C. J., Driscoll, J. F., Reuss, D. L., Drake, M. C., and Rosalik, M. E., 1998, "Vorticity Generation and Attenuation as Vortices Convect Through a Premixed Flame," *Combustion and Flame*, Vol. 112, No. 3,

pp. 342-358.

Mueller, C. J., and Schefer, R. W., 1998, "Coupling of a Diffusion Flame Structure to an Unsteady Vortical Flowfield," accepted for publication in *Twenty-Seventh Symposium (International) on Combustion*, The Combustion Institute, Pittsburgh.

Najm, H. N., Paul, P. H., Mueller, C. J., and Wyckoff, P. S., 1998, "On the Adequacy of Certain Experimental Observables as Measurements of Flame Burning Rate," *Combustion and Flame*, Vol. 113, No. 3, pp. 312-332.

Nguyen, Q.-V., and Paul, P. H., 1996, "The Time Evolution of a Vortex-Flame Interaction Observed via Planar Imaging of CH and OH," *Twenty-Sixth Symposium (International) on Combustion*, The Combustion Institute, Pittsburgh, pp. 357-364.

Nye, D. A., Lee, J. G., Lee, T.-W., and Santavicca, D. A., 1996, "Flame Stretch Measurements During the Interaction of Premixed Flames and Karman Vortex Streets Using PIV," *Combustion and Flame*, Vol. 94, No. 1/2, pp. 167-176.

Renard, P.-H., Rolon, J. C., Thevenin, D., and Candel, S., 1998a, "Wrinkling, Pocket Formation and Double Premixed Flame Interaction Processes," accepted for publication in *Twenty-Seventh Symposium (International) on Combustion*, The Combustion Institute, Pittsburgh.

Renard, P.-H., Rolon, J. C., Thevenin, D., and Candel, S., 1998b, "Investigations of Heat Release, Extinction, and Time Evolution of the Flame Surface for a Non-Premixed Flame Interacting with a Vortex," accepted for publication, *Combustion and Flame*.

Roberts, W. L., and Driscoll, J. F., 1991, "A Laminar Vortex Interacting with a Premixed Flame: Measured Formation of Pockets of Reactants," *Combustion and Flame*, Vol. 87, No. 3/4, pp. 245-256.

Roberts, W. L., 1992, "A Premixed Laminar Flame Interacting With a Vortex Resulting in Flame Stretch and Quenching," Ph.D. Dissertation, University of Michigan, Ann Arbor.

Roberts, W. L., Driscoll, J. F., Drake, M. C., and Ratcliffe, J. W., 1992, "OH Fluorescence Images of the Quenching of a Premixed Flame During an Interaction with a Vortex," *Twenty-Fourth Symposium (International) on Combustion*, The Combustion Institute, Pittsburgh, pp. 169-176.

Roberts, W. L., Driscoll, J. F., Drake, M. C., and Goss, L. P., 1993, "Images of the Quenching of a Flame by a Vortex – To Quantify Regimes of Turbulent Combustion," *Combustion and Flame*, Vol. 94, No. 1/2, pp. 58-69.

Rolon, J. C., Aguerre, F., and Candel, S., 1995, "Experiments on the Interaction Between a Vortex and a Strained Diffusion Flame," *Combustion and Flame*, Vol. 100, No. 3, pp. 422-429.

Samaniego, J.-M., 1992a, "Generation of Two-Dimensional Vortices in a Cross Flow," *Annual Research Briefs – 1992*, Center for Turbulence Research, NASA Ames Research Center/Stanford University, pp. 431-441.

Samaniego, J.-M., 1992b, "Stretch-Induced Quenching in Vortex-Flame Interactions," *Annual Research Briefs – 1993*, Center For Turbulence Research, NASA Ames Research Center/Stanford University, pp. 205-218.

Schauer, F. R., 1998, "Thermal Diffusion and Flame Structure in a Laminar Hydrogen Jet Diffusion Flame," Ph.D. Thesis, University of Illinois, Urbana.

Schauer, F. R., Hancock, R. D., Gogineni, S., and Lucht, R. P., 1998, "Vortex-Flame Interactions in Hydrogen Jet Diffusion Flames: A DPIV and DNS Investigation," submitted to *Experiments in Fluids*.

Sinibaldi, J. O., Mueller, C. J., Driscoll, J. F., 1997, "Measured Local Propagation Velocities of Wrinkled Premixed Flames," Proceedings of the *Fall Technical Meeting*, The Eastern States Section of the Combustion Institute, Hartford, CT, pp. 179-182.

Sinibaldi, J. O., Mueller, C. J., and Driscoll, J. F., 1998, "Local Flame Propagation Speeds Along Wrinkled, Unsteady, Stretched Premixed Flames," accepted for publication in *Twenty-Seventh Symposium (International) on Combustion*, The Combustion Institute, Pittsburgh.

Sullivan, J. P., Widnall, S. E., and Ezekiel, S., 1973a, "Study of Vortex Rings Using a Laser Doppler Velocimeter," AIAA Paper No. 73-105.

Sullivan, J. P., Widnall, S. E., and Ezekiel, S., 1973b, "Study of Vortex Rings Using a Laser Doppler Velocimeter," *AIAA Journal*, Vol. 11, No. 10, pp. 1384-1389.

Takagi, T., Yoshikawa, Y., Yoshida, K., Komiyama, M., and Kinoshita, S., 1996, "Studies on Strained Non-Premixed Flames Affected by Flame Curvature and Preferential Diffusion," Twenty-Sixth Symposium (International) on Combustion, The Combustion Institute, Pittsburgh, PA, pp. 1103-1110.

Thevenin, D., Rolon, J. C., Renard, P.-H., Kendrick, D. W., Veynante, D., and Candel, S., 1996, "Structure of a Nonpremixed Flame Interacting with Counterrotating Vortices," *Twenth-Sixth Symposium (International) on Combustion*, The Combustion Institute, Pittsburgh, pp. 1079-1086.

Thevenin, D., Renard, P.-H., Rolon, J. C., and Candel, S., 1998, "Extinction Processes During a Non-Premixed Flame/Vortex Interaction," accepted for publication in *Twenty-Seventh Symposium (International) on Combustion*, The Combustion Institute, Pittsburgh.

Trieling, R. R., Beckers, M., and van Heijst, G. J. F., 1997, "Dynamics of Monopolar Vortices in a Strain Flow," *Journal of Fluid Mechanics*, Vol. 345, pp. 165-201.

Trieling, R. R., van Wesenbeeck, J. M. A., and van Heijst, G. J. F., 1998, "Dipolar Vortices in a Strain Flow," *Physics of Fluids*, Vol. 10, No. 1, pp. 144-159.

Yoshida, K., and Takagi, T., 1998, "Transient Local Extinction and Reignition Behavior of Diffusion Flames Affected by Flame Curvature and Preferential Diffusion," accepted for publication in *Twenty-Seventh Symposium (International) on Combustion*, The Combustion Institute, Pittsburgh.

Widnall, S. E., 1975, "The Structure and Dynamics of Vortex Filaments," *Annu. Rev. Fluid. Mech.*, Vol. 7, pp. 141-165.

List of multimedia data

1) Animation AB082_1.mov, Acetone PLIF sequence (movie of color pictures, 154 kB)
2) Animation AB082_2.mov, OH PLIF sequence without extinction (movie of color pictures, 490 kB)
3) Animation AB083_3.mov, OH PLIF sequence with annular extinction (movie of color pictures, 436 kB)
4) Animation AB084_4.mov, OH PLIF sequence with annular extinction (movie of color pictures, 193 kB)

Movie 1 Acetone PLIF sequence

Movie 2 OH PLIF sequence without extinction

Movie 3 OH PLIF sequence with annular extinction

Movie 4 OH PLIF sequence with annular extinction